# Four-wheel Driving-force Distribution Method for Instantaneous or Split Slippery Roads for Electric Vehicle with In-wheel Motors

Kenta Maeda, Hiroshi Fujimoto and Yoichi Hori
The University of Tokyo
5-1-5 Kashiwanoha, Kashiwa, Chiba, Japan
Email: maeda@hflab.k.u-tokyo.ac.jp, fujimoto@k.u-tokyo.ac.jp, hori@k.u-tokyo.ac.jp

***Abstract*—In this paper, a four-wheel driving force distribution method based on driving force control is proposed. Driving force control is a traction control method, previously proposed by the authors' research group, which generate appropriate driving force based on the acceleration pedal. However, this control method can not completely prevent reduction of driving force when a vehicle runs on an extremely slippery road. If the length of a slippery surface is shorter than the vehicle's wheel base, the total driving force is retained by distributing the shortage of driving force to the wheels that still have traction. On the other hand, when either the left or right side runs on a slippery surface, yaw-moment is suppressed by setting total driving forces of left and right wheels to be the same. Therefore, four-wheel driving force distribution method is proposed for retaining driving force on instantaneous slippery roads, and suppressing yaw-moment on split ones. The effectiveness of the proposed distribution method is verified by simulations and experiments.**

## I. Introduction

As a solution for energy and environmental problems, electric vehicles (EVs) are receiving great attention. In addition, EVs have many advantages over internal combustion engine vehicles, since electric motors and inverters are utilized in EV drive systems. Their advantages can be summarized as follows [1]:

1) The torque response of electric motors is 100–500 times faster than that of engines.
2) All wheels can be controlled independently by adopting small high-power in-wheel motors.
3) The output torque of an electric motor can be measured accurately from the motor current.

Based on these advantages, many traction control methods [2], [3], [4] and motion stabilization control methods [5], [6] have been proposed.

The authors' research group has previously proposed driving force control (DFC) [7] as a new method of traction control. DFC is a control method that directly controls driving force with driving force outer loop based on driving force observer, and wheel-speed inner loop based on slip ratio control [8], which can generate large yet uncertain driving force on slippery roads. With this control system, the desired driving force is generated within the saturator limits, and traction is retained by slip ratio control when the driving force saturates. Moreover, driving force commanded by a driver can be generated by using the acceleration pedal as the driving force reference.

Fig. 1. FPEV2-Kanon.

Fig. 2. In-wheel motor.

Since DFC proposed in [7] is considered for front-wheel-driven EVs, it is inevitable that total driving force diminishes on extremely slippery roads. However, sudden decrease of driving force leads to driver discomfort, and thus a novel control method is needed to retain total driving force. In addition, the left and right driving forces need to be equal to prevent yawing.

In this paper, a four-wheel driving force distribution method based on DFC is proposed for EV with in-wheel motors. As mentioned, it is one of EVs' advantages that all-wheel-drive vehicles can easily be realized by adopting small high-power in-wheel motors. Even when a vehicle runs into a slippery road such as scattered snow or wet manholes, whose length is shorter than the vehicle's wheel base, total driving force is retained by distributing the shortage of driving force to wheels that still have traction. Additionally, when either left or right side are on a slippery surface, yawing is suppressed by generating the difference between left and right driving force to follow desired yaw-moment — zero when running straight. The four-wheel driving force distribution method proposed in this paper can realize both functions simultaneously. The effectiveness of the proposed method is verified by simulations and experiments.

## II. Experimental Vehicle

The experimental EV "FPEV2-Kanon," developed by the authors' laboratory, is used for performance verification as shown in Fig. 1. In this section the characteristics of the experimental vehicle are explained.

Outer-rotor-type in-wheel motors as shown in Fig. 2 are installed in each wheel. Since these motors adopt direct drive

TABLE I
VEHICLE SPECIFICATIONS.

| | |
|---|---|
| Vehicle Mass ($m$) | 870 [kg] |
| Wheel Base ($l$) | 1.7 [m] |
| Distance from C.G to Fromt Axle ($l_f$) | 0.999 [m] |
| Distance from C.G to Rear Axle ($l_r$) | 0.701 [m] |
| Tread Base ($d_f$, $d_r$) | 1.3 [m] |
| Wheel Radius ($r$) | 0.302 [m] |

system, reaction forces from roads are directly transferred to the motors without gear reduction or backlash. The maximum torque of each of the front motors is $\pm 500$ [Nm], and that of the rear is $\pm 340$ [Nm]. Additionally, an optical sensor is installed to measure the vehicle velocity accurately. The vehicle's specification is shown in Table I.

## III. EQUATIONS OF VEHICLE DYNAMICS

In this section, equations of vehicle dynamics are explained [7].

The equation of rotational motion of each wheel is shown in Fig. 3 and can be described as

$$J_{ij}\dot{\omega}_{ij} = T_{ij} - rF_{dij}, \tag{1}$$

where $J$ is the wheel inertia, $\omega$ is the wheel angular velocity, $T$ is the motor torque, $r$ is the wheel radius, $F_d$ is the driving force at the point where the wheel makes contact with the ground. Also, $i$ and $j$ are indices for $f/r$ (front/rear) and $l/r$ (left/right) respectively. The equation of longitudinal motion of the vehicle body is shown in Fig. 4 and can be described as

$$m\dot{V} = F_{dfl} + F_{dfr} + F_{drl} + F_{drr}, \tag{2}$$

where $m$ is the vehicle mass, $V$ is the vehicle velocity. When the vehicle accelerates or decelerates, the wheel velocity $V_\omega = r\omega$ differs from the vehicle velocity $V$. The slip ratio $\lambda$ is defined as

$$\lambda = \frac{V_\omega - V}{\max(V_\omega, V, \epsilon)}, \tag{3}$$

where $\epsilon$ is a tiny value to prevent division by zero. The driving force $F_d$ and the driving stiffness $D_s$ at each wheel are obtained as

$$F_{dij} = \mu_{ij} N_{ij}, \tag{4}$$

$$D_{sij} = \left.\frac{dF_{dij}}{d\lambda_{ij}}\right|_{\lambda_{ij}=0}, \tag{5}$$

where $N$ is the normal reaction force on each wheel, and $\mu$ is the friction coefficient.

The relationship between $\mu$ and $\lambda$ depends on the road condition, and is known to be as Fig. 5 [9]. There are $\lambda_{\mathrm{peak,p}}$, $\lambda_{\mathrm{peak,n}}$ on which $\mu$ is the maximum or the minimum. In the domain of $\lambda_{\mathrm{peak,n}} \le \lambda \le \lambda_{\mathrm{peak,p}}$, $\mu$ is a monotonically increasing function of $\lambda$, and outside the domain, a monotonically decreasing function.

## IV. DRIVING FORCE CONTROL

### A. Driving Force Control

In this section, the driving force control (DFC) method is explained [7]. The block diagram of DFC is shown in Fig. 6. The outer loop is a driving force loop based on driving force observer and the inner loop is a wheel velocity loop that controls the slip ratio. $F_d^*$ is the driving force reference and $\hat{F}_d$ is the estimated driving force.

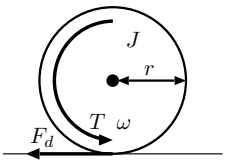


Fig. 3. Rotational motion of wheel.

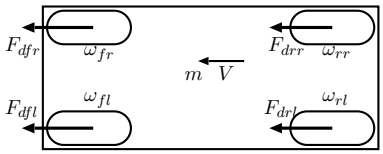


Fig. 4. Variables in vehicle motion.

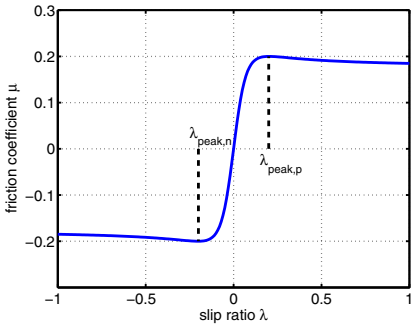


Fig. 5. Typical $\mu$-$\lambda$ relationship.

Since the definition of slip ratio $\lambda$ for acceleration ($V_\omega \ge V$) differs from that of the definition for deceleration ($V_\omega < V$), $\lambda$ is inconvenient to control. Therefore, instead of the slip ratio, the control input $y$, defined as follows, is controlled.

$$y = \frac{V_\omega}{V} - 1. \tag{6}$$

This is the same definition as the definition of slip ratio for deceleration. The relationship between $\lambda$ and $y$ in the domain of $\lambda > 0$ is calculated as

$$y = \frac{\lambda}{1-\lambda}, \tag{7}$$

which indicates that $y$ equals to $\lambda$ when $|\lambda| \ll 1$ and they are always one to one correspondence.

From (6), the wheel velocity reference $V_\omega^*$ of the inner loop is calculated as

$$V_\omega^* = (1+y)V, \tag{8}$$

which shows that the vehicle can not start moving when at rest ($V = 0$) since $V_\omega^*$ is equal to 0 independent of $y$. To prevent this problem, the reference $V_\omega^*$ is modified where $V$ is smaller than a given constant $\sigma$ as shown in (9).

$$\begin{cases} V_\omega^* = V + y\sigma & (V < \sigma), \\ V_\omega^* = V + yV & (V \ge \sigma). \end{cases} \tag{9}$$

From (5), it can be considered that $F_d \simeq D_s\lambda$ provided that $|\lambda| \ll 1$. In addition, assuming that wheel velocity control is fast enough to be $y \simeq \lambda$, the transfer function from $y$ to $F_d$ is assumed to be zero order as

$$F_d = D_s\lambda \simeq D_s y. \tag{10}$$

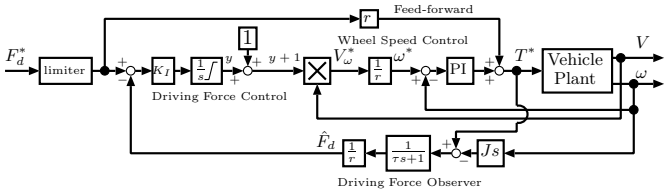


Fig. 6. Block diagram of DFC.

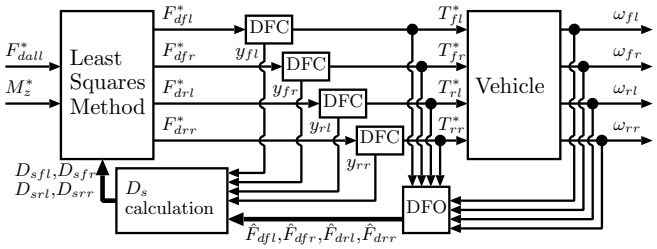


Fig. 7. The block diagram of proposed method.

Therefore, the driving force controller is set as I control with gain $K_I$, whose initial value is set as $y_0 = 0$. Saturation is applied to the integrator output for limiting $y$ to $y_{\min} \leq y \leq y_{\max}$. With this saturation, traction can be retained by keeping the slip ratio within the domain where $\mu$ is monotonic function of $\lambda$.

In Fig. 6, feed-forward to motor torque reference $T^*$ is obtained by adding $rF_d^*$, which is added anew in this paper in order to improve response speed. If the wheel has traction, then $T_{ij} \simeq rF_{dij}$ holds, since $J_{ij}\dot{\omega_{ij}}$ is assumed to be small in (1). Therefore, due to the feed-forward, the system can generate approximate driving force, and slight differences are compensated for by the driving force feed-back. Also, when a wheel is on a slippery surface, traction is maintained due to feed-back.

### *B. Driving Force Observer*

In this section, the driving force observer (DFO) is explained.

$J$ and $r$ are given in (1), and $\omega$ can be measured. Moreover, the motor torque $T$ can be controlled accurately. Therefore, with the DFO shown in the bottom of Fig. 6, the driving force $F_d$ at each wheel can be estimated with motor torque reference $T^*$ and wheel velocity $\omega$, assuming that current control of motor is fast enough for $T = T^*$ to be valid. $\tau$ is the time constant of the DFO.

## V. Proposed Driving Force Distribution Method

In this section, the proposed method of four-wheel driving force distribution is explained. When the control input $y$ of DFC approaches the upper limit, driving force is saturated and reduced. To avoid this reduction, $y$ of each wheel need to be small enough to prevent saturation. Therefore, the proposed method decides the driving force reference of each wheel to minimize $y$ of each wheel, satisfying total driving force reference $F_{dall}^*$ and yaw-moment reference $M_z^*$ generated by driving force difference.

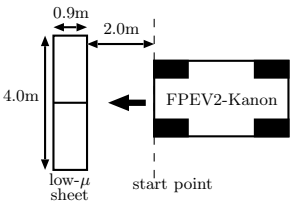


Fig. 8. Instantaneous low-$\mu$ road.

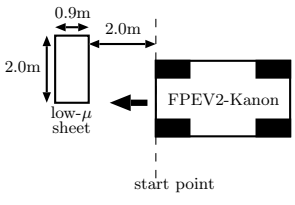


Fig. 9. Split low-$\mu$ road.

The relationship between driving force of each wheel $F_{dij}$ and $F_{dall}$, $M_z$ is as follows:

$$\begin{bmatrix} 1 & 1 & 1 & 1 \\ -\frac{d_f}{2} & \frac{d_f}{2} & -\frac{d_r}{2} & \frac{d_r}{2} \end{bmatrix} \begin{bmatrix} F_{dfl} \\ F_{dfr} \\ F_{drl} \\ F_{drr} \end{bmatrix} = \begin{bmatrix} F_{dall} \\ M_z \end{bmatrix}. \quad (11)$$

Here, by setting the coefficient matrix in the left-hand side as $\boldsymbol{A}$, the vector of driving force of each wheel $[F_{dfl}, F_{dfr}, F_{drl}, F_{drr}]^T$ as $\boldsymbol{x}$, and that of total driving force and yaw-moment $[F_{dall}, M_z]^T$ as $\boldsymbol{b}$, (11) can be re]written as $\boldsymbol{Ax} = \boldsymbol{b}$. From (10) driving stiffness of each wheel $D_{sij}$ can be obtained as

$$D_{sij} = \frac{F_{dij}}{y_{ij}}. \quad (12)$$

Then the cost function $J$ is defined as the sum of squares of the DFC control inputs $y_{ij}$.

$$\begin{aligned} J &= y_{fl}^2 + y_{fr}^2 + y_{rl}^2 + y_{rr}^2 \\ &= \frac{F_{dfl}^2}{D_{sfl}^2} + \frac{F_{dfr}^2}{D_{sfr}^2} + \frac{F_{drl}^2}{D_{srl}^2} + \frac{F_{drr}^2}{D_{srr}^2}. \end{aligned} \quad (13)$$

Therefore, the weighted least squares solution $\boldsymbol{x_{opt}}$ of (11) that minimizes $J$, and weighting matrix $\boldsymbol{W}$ are as follows.

$$\boldsymbol{x_{opt}} = \boldsymbol{W}^{-1}\boldsymbol{A}^T(\boldsymbol{A}\boldsymbol{W}^{-1}\boldsymbol{A}^T)^{-1}\boldsymbol{b}, \quad (14)$$

$$\boldsymbol{W} = \mathrm{diag}\left(\frac{1}{D_{sfl}^2}, \frac{1}{D_{sfr}^2}, \frac{1}{D_{srl}^2}, \frac{1}{D_{srr}^2}\right). \quad (15)$$

Fig. 7 shows the block diagram of the whole system. The driving force references $F_{dij}^*$ are given by $\boldsymbol{x_{opt}}$ and the driving stiffness of each wheel $D_{sij}$ is calculated by the following equation.

$$D_{sij} = \frac{\hat{F}_{dij}}{y_{ij}}, \quad (16)$$

where $\hat{F}_{dij}$ is the estimated driving force of each wheel. Lower limitations 0.005 and 50 are imposed to $y_{ij}$ and $\hat{F}_{dij}$ in (16) respectively, avoiding division by zero both in (11) and (16). Therefore, in the region where $\hat{F}_{dij}$ and $y_{ij}$ are small, $D_s$ is set to be 10000, which corresponds to the high-$\mu$ surface with friction coefficient $\mu$ of about 0.8 when the slip ratio $\lambda$ is 0.2. The response speed of driving force distribution depends on the calculation speed of $D_s$, i.e. the integrator gain $K_I$ of DFC.

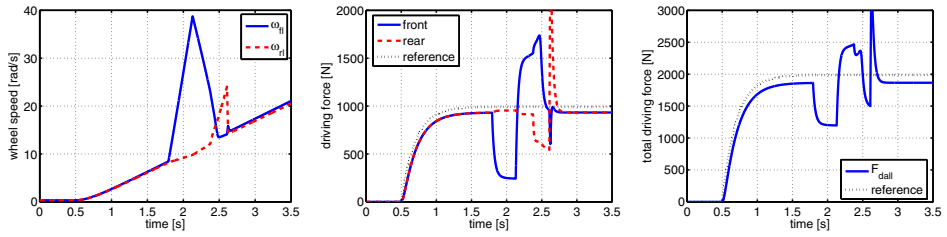


(a) $\omega_{fl}$, $\omega_{rl}$ (b) $\hat{F}_{df}$, $\hat{F}_{dr}$ (c) $\hat{F}_{dall}$

Fig. 10. Simulation of instantaneous slippery road (without control)

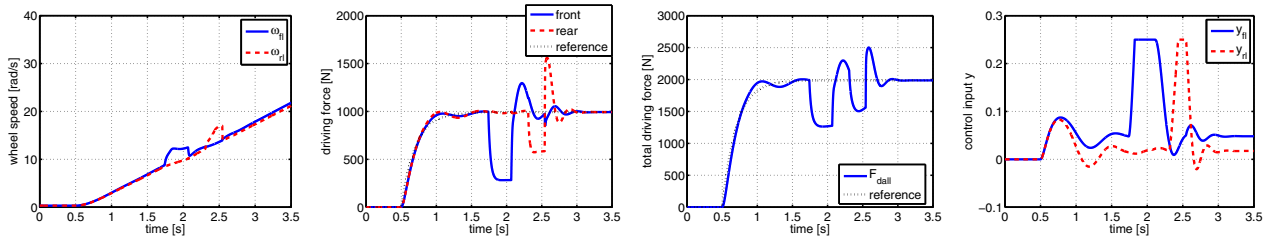


(a) $\omega_{fl}$, $\omega_{rl}$ (b) $\hat{F}_{df}$, $\hat{F}_{dr}$ (c) $\hat{F}_{dall}$ (d) $y_{fl}$, $y_{fr}$

Fig. 11. Simulation of instantaneous slippery road (only DFC)

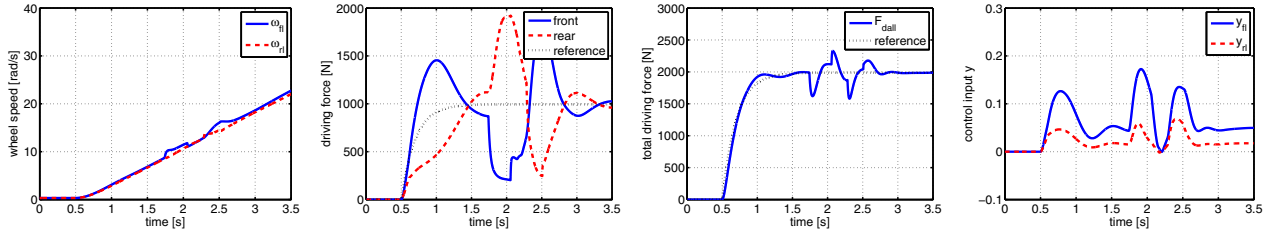


(a) $\omega_{fl}$, $\omega_{rl}$ (b) $\hat{F}_{df}$, $\hat{F}_{dr}$ (c) $\hat{F}_{dall}$ (d) $y_{fl}$, $y_{fr}$

Fig. 12. Simulation of instantaneous slippery road (proposed)

## VI. Simulation

### A. Instantaneous Slippery Road

In this section, simulation results of acceleration on an instantaneous slippery road are explained. As shown in Fig. 8, an extremely low $\mu$ road of $\mu = 0.1$ of length 0.9 [m], shorter than the wheel base of "FPEV2-Kanon", is set at the distance of 2.0 [m] from the start point.

The experimental vehicle starts at the start point and acceleratez with total driving force reference $F^*_{dall} = 600/r = 1993.4$ [Nm]. The parameters are, $K_I = 0.01$, $\tau = 30$ [ms], $y_{\max} = 0.25$ which corresponds to a slip ratio of $\lambda = 0.2$. The wheel speed PI controller is designed by the pole assignment method towards the plant $\frac{1}{Js}$, which is from (1) ignoring $F_d$, setting the pole $-20$ [rad/s]. All parameters are the same for each wheel.

The simulation results are shown in Fig. 10–12. In this paper, without control means generating constant motor torque of 150 [Nm] on each wheel. Without control, extreme slip occurs in Fig. 10(a) then the driving force decreases in Fig. 10(b), 10(c). With only DFC, although the traction is obtained in Fig. 10(a), the driving force decreases in Fig. 11(b), 11(c), similar to the case without control. In contrast, with the proposed method, Fig. 12(b) shows that the driving force on each wheel is distributed to retain total driving force as shown in Fig. 12(c), as well as the traction shown in Fig. 12(a). In addition, comparing with Fig. 11(d), Fig. 12(d) shows that the proposed method prevents the satulation of $y$.

### B. Split Slippery Road

In this section, simulation results of acceleration on a split slippery road are explained. The low-$\mu$ road is set as shown in Fig. 9. The parameters and other conditions are the same as explained in the previous section.

The simulation results are shown in Fig. 13, 14. With only DFC, Fig. 13(a) shows that the driving force in only the right wheels reduce. In contrast, with the proposed method, driving force of each wheel is distributed as shown in Fig. 14(a) to retain driving force while preventing the generation of yaw-moment, which can be confirmed by comparing Fig. 13(b), 13(c) with Fig. 14(b), 14(c).

## VII. Experiments

### A. Instantaneous Slippery Road

In this section, experimental results on an instantaneous slippery road are explained under the same condition as the simulation in sec. VI-A, however the front and rear motor torque is limited to 300 [Nm], 220 [Nm] for ensuring safety inside the university. A polymer sheet is used for a slippery road. This sheet, called "low-$\mu$ sheet" in this paper, can realize a low $\mu$ road of about $\mu = 0.2$ by watering on it.

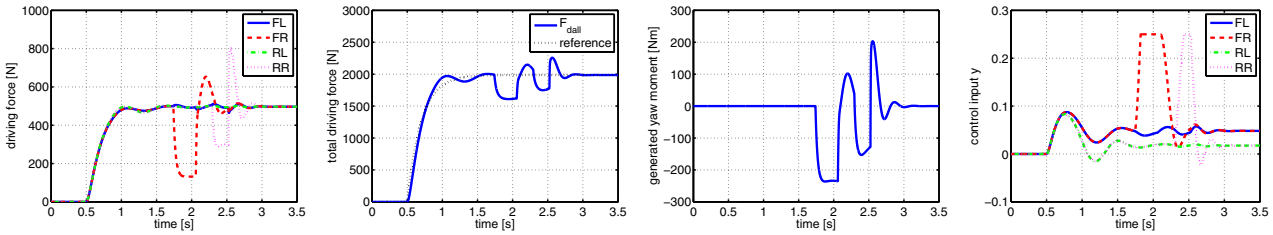


(a) $\hat{F}_d$ on each wheel (b) $\hat{F}_{dall}$ (c) $\hat{M}_z$ (d) $y$ on each wheel

Fig. 13. Simulation of split slippery road (only DFC)

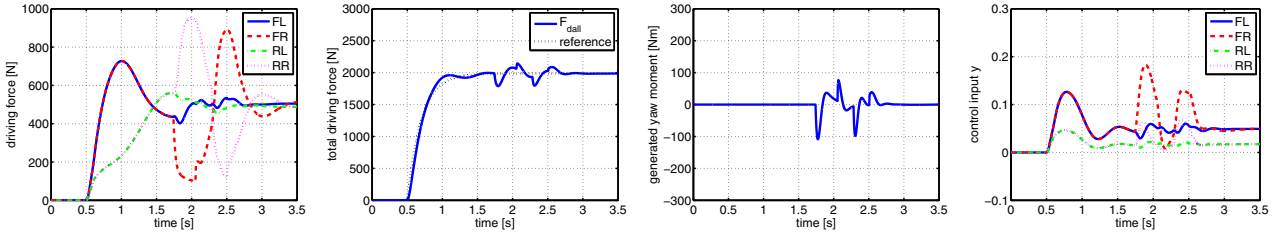


(a) $\hat{F}_d$ on each wheel (b) $\hat{F}_{dall}$ (c) $\hat{M}_z$ (d) $y$ on each wheel

Fig. 14. Simulation of split slippery road (proposed)

The experimental results are shown in Fig. 15–17. Comparing Fig. 15(a) with Fig. 16(a), 17(a), traction is obtained by DFC. As for driving force, without control and with only DFC, driving force decreases in Fig. 15(b), 15(c), 16(b), 16(c), similar to the simulation results. In contrast, with the proposed method, Fig. 17(b) shows that driving force on each wheel is distributed to retain total driving force as shown in Fig. 17(c). The total driving force slightly decrease when front wheels are on the slippery road from 1.7 [s] to 2.2 [s] because the motor torque of rear motors approach the upper limit.

Additionaly, comparing with Fig. 16(d), Fig. 17(d) shows that the proposed method prevents the satulation of $y$ when the front wheels are on the slippery road.

### *B. Split Slippery Road*

In this section, experimental results on a split slippery road are explained under the same condition as the simulation in sec. VI-B. The results are shown in Fig. 18, 19. With only DFC, Fig. 18(a) shows that only right wheels reduce their driving forces. In contrast, with the proposed method, driving force of each wheel is distributed as shown in Fig. 19(a) to retain driving force and prevent the generation of yaw-moment, which can be confirmed by comparing Fig. 18(b), 18(c) with Fig. 19(b), 19(c).

## VIII. Conclusion

In this paper, four-wheel driving force distribution method for instantaneous or split slippery roads is proposed, and its effectiveness is verified by simulations and experiments. With the proposed distribution method, the reduction of total driving force and generation of yaw-moment is prevented. Therefore EVs can be driven without difficulty no matter what road condition.

In future, the authors' research group plans to consider deceleration and cornering, and to estimate $\lambda_{\mathrm{peak}}$ in realtime based on DFC.


## Acknowledgment

This research was partly supported by the Industrial Technology Research Grant Program from the New Energy and Industrial Technology Development Organization (NEDO) of Japan, and by the Ministry of Education, Culture, Sports, Science and Technology grant number 22246057. Additionally, attendance at AMC12 is supported by IEEJ International Conference Travel Grant.


## References


[1] Y.Hori: "Future vehicle driven by electricity and control—research on four-wheel-motored "UOT Electric March II"", *IEEE Trans. Industrial Electronics*, Vol.51, No.5, pp.954–962 (2004)

[2] D.Yin, Y.Hori: "A new approach to traction control of EV based on maximum effective torque estimation", in *Proc. the 34th Annual Conference of the IEEE Industrial Electronics Society*, pp.2764–2769 (2008)

[3] D.Foito, M.Guerreiro, A.Cordeiro : "Anti-slip wheel controller drive for EV using speed and torque observers", in *Proc. the 18th International Conference on Electrical Machines*, pp.1–5 (2008)

[4] Yinghui Ge, C.S.Chang : "Torque distribution control for electric vehicle based on traction force observer", in *Proc. the IEEE International Conference on Computer Science and Automation Engineering*, pp.371–375 (2011)

[5] H.Ogura, T.Murakami: "Improvement of vehicle stability by reaction force control on accelerator pedal and steering wheel", in Proc. International Power Electronics Conference, pp.2956–2963 (2010)

[6] M.Kamachi, K.Walters: "A research of direct yaw-moment control on slippery road for in-wheel motor vehicle", in *Proc. International Battery, Hybrid and Fuel Electric Vehicle Symposium*, pp.2122–2133 (2006)

[7] M.Yoshimura, H.Fujimoto: "Driving torque control method for electric vehicle with in-wheel motors", *IEEJ Trans. Industry Applications*, Vol.131, No.5, pp.1-8 (2010) (in Japanese)

[8] T.Suzuki, H.Fujimoto: "Slip ratio estimation and regenerative brake control without detection of vehicle velocity and acceleration for electric vehicle at urgent brake-turning", in *Proc. the 11th IEEE International Workshop on Advanced Motion Control*, pp.273–278 (2010)

[9] H.B.Pacejka, E.Bakker: "The magic formula tyre model", Tyre models for vehicle dynamic analysis: in *Proc. the 1st International Colloquium on Tyre Models for Vehicle Dynamics Analysis*, held in Delft, The Netherlands (1991)

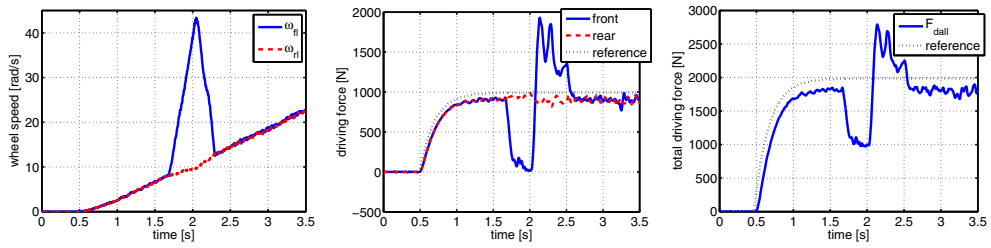


(a) $\omega_{fl}$, $\omega_{rl}$ (b) $\hat{F}_{df}$, $\hat{F}_{dr}$ (c) $\hat{F}_{dall}$

Fig. 15. Experiment of instantaneous slippery road (without control)

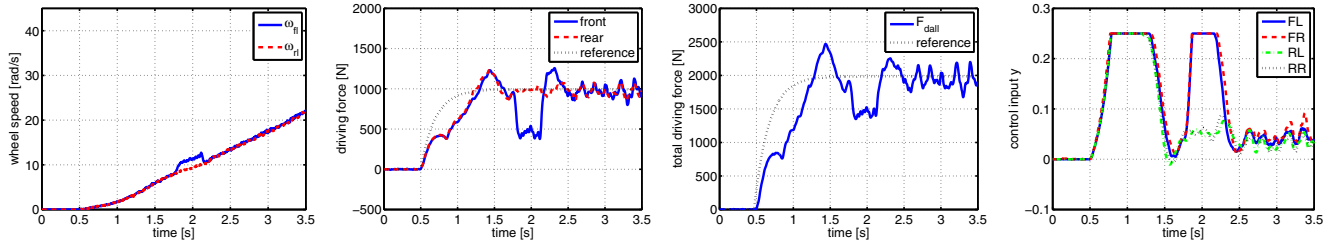


(a) $\omega_{fl}$, $\omega_{rl}$ (b) $\hat{F}_{df}$, $\hat{F}_{dr}$ (c) $\hat{F}_{dall}$ (d) $y_{fl}$, $y_{fr}$

Fig. 16. Experiment of instantaneous slippery road (only DFC)

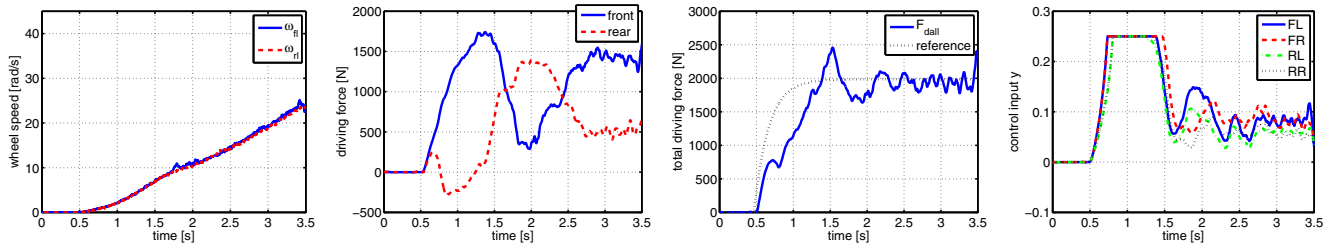


(a) $\omega_{fl}$, $\omega_{rl}$ (b) $\hat{F}_{df}$, $\hat{F}_{dr}$ (c) $\hat{F}_{dall}$ (d) $y_{fl}$, $y_{fr}$

Fig. 17. Experiment of instantaneous slippery road (proposed)

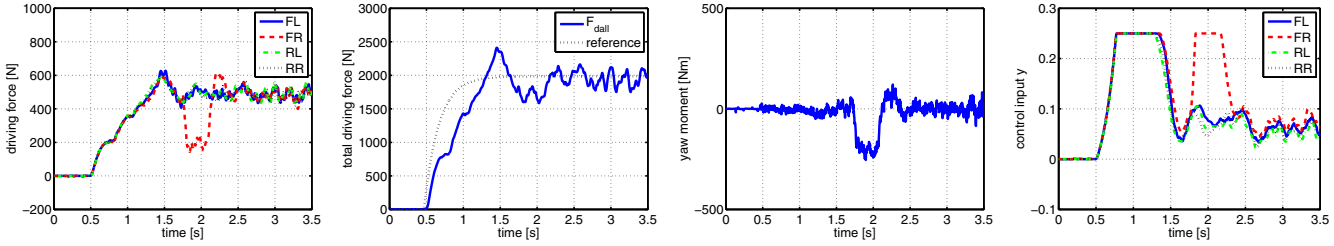


(a) $\hat{F}_d$ on each wheel (b) $\hat{F}_{dall}$ (c) $\hat{M}_z$ (d) $y$ on each wheel

Fig. 18. Experiment of split slippery road (only DFC)

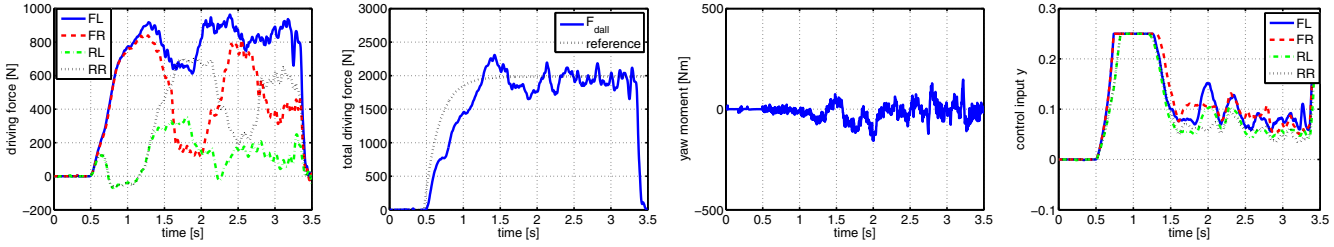


(a) $\hat{F}_d$ on each wheel (b) $\hat{F}_{dall}$ (c) $\hat{M}_z$ (d) $y$ on each wheel

Fig. 19. Experiment of split slippery road (proposed)